Nanoprecision algorithm for surface plasmon resonance determination from images with low contrast for improved se....

Article *in* Journal of Nanophotonics · June 2011

DOI: 10.1117/1.3598138

CITATIONS
20

READS
220

3 authors, including:

Alina Karabchevsky
Ben-Gurion University of the Negev
55 PUBLICATIONS **275** CITATIONS
SEE PROFILE

Ibrahim Abdulhalim
Ben-Gurion University of the Negev
237 PUBLICATIONS **3,081** CITATIONS
SEE PROFILE

Journal of Nanophotonics

SPIEDigitalLibrary.org/jnp

Nanoprecision algorithm for surface plasmon resonance determination from images with low contrast for improved sensor resolution

Alina Karabchevsky
Serge Karabchevsky
Ibrahim Abdulhalim

SPIE

Nanoprecision algorithm for surface plasmon resonance determination from images with low contrast for improved sensor resolution

Alina Karabchevsky, Serge Karabchevsky, and Ibrahim Abdulhalim
Ben Gurion University, Department of Electro-optic Engineering, Beer Sheva 84105, Israel
rudenko@bgu.ac.il

Abstract. A forward-projection algorithm based on Radon transform for two-dimensional surface plasmon imaging was devised to achieve nanoscale precision in determining the surface plasmon signal. A diverging laser beam at the chosen frequency was used to overcome the angular scanning in the well-known Kretschmann configuration. Multichannel sensing with improved resolution was realized. The technique was also used to find the lateral resolution of the sensor using a patterned layer of 40-nm thick SiO_2 layer on top of the metallic surface. As a surface plasmon resonance signal detector, the use of the proposed Radon transform algorithm shows nanoprecision accuracy in cases of single and multichannel sensing. The method also provides the filtered output of the signal without any extra modification and therefore, it is nonsensitive to noise. [DOI: 10.1117/1.3598138]

Keywords: surface plasmon resonance; nanophotonics; biosensing; curve fit; peak extraction; Radon transform; background suppression; forward projection.

Paper 11018SSR received Jan. 30, 2011; revised manuscript received May 2, 2011; accepted for publication May 16, 2011; published online Jun. 23, 2011.

1 Introduction

Determination of the surface plasmon resonance (SPR) location with high accuracy is of major importance for improving the sensor resolution. In many applications, it is of great interest to accurately detect and measure the position of an extremum in an electrical signal.[1] For example, a correlation process produces an output having a peak at a position related to the phase difference of its inputs. In image processing, communications, and digital signal processing, the detection of peaks and their positions is often necessary. In the plasmonics field, however, SPR sensing has become an undisputable leading technology. The main benefit of the SPR is label-free detection and studies of biological binding to the sensor surface.[2]

1.1 A Review of Different Approaches

The most popular SPR sensing scheme uses the prism coupling in the Kretschmann–Raether (KR) arrangement.[3] In the KR configuration, reflectivity is measured as a function of angle of incidence, called angular modulation (AM), or wavelength, called wavelength modulation. In the AM a single wavelength, usually a collimated laser beam, is incident on the metal film through the prism while scanning through different incidence angles. The SPR dip is observed in the reflectivity versus incidence angle spectrum. Although the AM uses a single frequency and a collimated beam, the required scanning is problematic, in particular when high accuracy

1934-2608/2011/$25.00

and fast speed are required. Using an imaging scheme, the possibility of detecting arrays or imaging surfaces with very low contrast was demonstrated.[4–6]

One of the SPR data analysis approaches is minimal hunt method[7] by fitting a similar function to a portion of the data surrounding the most attenuated wavelength (wavelength interrogation) or angle (angular interrogation) using an analytical derivative to find its minimum. Since the reflectivity response (versus angle or wavelength) is highly nonlinear, it is difficult to fit it analytically. An alternative to the minimum hunt technique is a straightforward application of a center-of-mass calculation, which was suggested by Jacobus and Chien[8] in their edge detection algorithm. The center-of-mass of the resulting resonant dip is directly dependent on the depth and width of the resonance because it is an asymmetric curve and, therefore, it is not a highly repeatable metric. Another data analysis method is the locally weighted parametric regression (LWPR)[9] which uses the regression technique to calibrate location-shifting signals such as those produced by SPR. The LWPR method has been developed for the calibration of wavelength-modulated SPR sensors. This calibration method combines LWPR and nonlinear principal components regression. It was shown that LWPR provides a calibration model that is more robust to random errors than traditional minima hunt calibration methods applied to SPR sensors.[9] Linearization of data processing algorithms and an optimal linear data analysis method were proposed as a means of optimizing algorithm parameters.[10] In our previous work,[11] we proposed a Radon transform-based algorithm to analyze the SPR noisy data, which is much simpler and straightforward than the existing methods. In this article,[11] we demonstrated a fast and accurate SPR sensor that overcomes the problems associated with mechanical scanning using a single frequency diverging beam combined with a camera and special processing algorithm that helps in reducing the effects of speckle noise. Diverging incidence laser beam contains a range of spatial frequencies (angles) that excite SPs (surface plasmons), causing the appearance of a dark line perpendicular to the surface wave propagation. Spatial frequency k of the incident light along the surface (k_x) defined as: $k_x = k_o \sin\theta_i$ with $k_o = 2\pi n/\lambda$ while n is the refractive index (RI) of the analyte. Therefore, during the article we will use both terms which are acceptable in SPR and imaging fields: spatial frequency or incidence angles. In the present article, we explain in detail the benefits of this method, which is based on the Radon transform integration behavior and propose a triple channel SPR detection algorithm.

2 Experimental

To demonstrate the concept presented in Sec 1.1, silver layers (70-nm thickness) were deposited on SF11 and BK7 glass slides. A thin layer of SiO_2 (~21 nm thickness) was deposited on top of the silver film for protection from oxidation. For the sensing elements (Ag deposited on glass substrate samples with or without anti-oxidation layer) on BK7, the FWHM is 0.3° in air with the SiO_2 layer. Note that the parameters of the sensing element are not ideal, which is preferable for our purpose to demonstrate the concept of improving the resolution even on a nonideal case. The samples were characterized first using the standard KR arrangement, while the incident laser beam at 637 nm was collimated. To perform the experiment with a diverging beam, the setup shown in Fig. 1 was used where the 637 nm laser diode is diverging, such that the beam incident on the prism cathetus has a diameter smaller than the cathetus width. The convex lens in front of the camera was added to collect the beam so that it fits the active area of the camera sensor. The sample is held on the base of the prism horizontally for convenience while adding liquids as shown on Fig. 1. Output images acquired by the camera were processed using MATLAB. The proposed setup is very useful for sensing applications in liquids since the prism and the sensing element are oriented horizontally, thus enabling dripping of the analyte on top of the sensing element into adhesive silicone isolator (Sigma product).

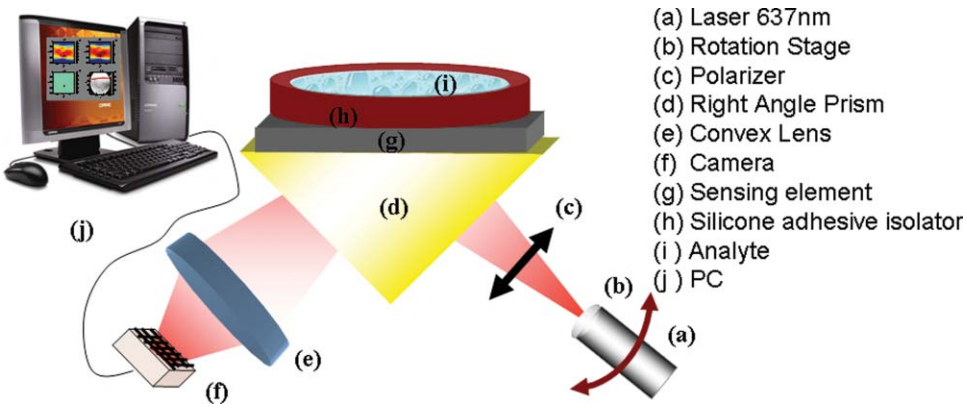

Fig. 1 Optical set-up.

3 Extraction Algorithms for Speckled Surface Plasmon Resonance Images

3.1 SPR Single Channel Extraction Algorithm

A speckle noise is a random intensity pattern produced by the interference of a set of random wave fronts, which produces a resultant wave whose amplitude, and therefore, intensity, varies randomly. In order to locate the SPR dark line in a highly speckled low contrast SPR image, we propose a Radon transform (RT)[12] [named after the Austrian mathematician Johann Radon (1917)] based algorithm which is not sensitive to the speckle noise. The RT in polar coordinates is defined as follows:[12]

$$(\Re f) \equiv g(\rho,\theta) = \int_{-\infty}^{\infty}\int_{-\infty}^{\infty} f(x,y)\delta(x\cos\theta + y\sin\theta - \rho)\,dx\,dy$$
$$= \int_{-\infty}^{\infty} f(\rho\cos\theta - l\sin\theta, \rho\sin\theta - l\cos\theta)dl, \quad (1)$$

where $f(x,y)$ is a two-dimensional function which represents the image, $\rho = \sqrt{x^2+y^2}$ and $\theta \in [-90^\circ, 90^\circ]$ are the radial the polar coordinates, respectively. The Dirac δ-function converts the two-dimensional integral to a line integral along the line: $x\cos\theta + y\sin\theta = \rho$; (x,y) are the pixel coordinates in the image: $x \in [0,m]$ and $y \in [0,n]$ with $m \times n$ being the dimensions of the camera sensor in pixels. To translate pixels to degrees, each coordinate should be multiplied by the angular pixel size. The function $f(x,y)$ represents unknown reflection from the sensing element, and then $g_{\min}(\rho,\theta)$ (in Radon space) represents the parameters of the SPR line at given analyte. Due to the integration along the line, RT is sensitive to line patterns. Since, in the case of the SPR imaging with diverged incident beam, excited SP produces a line-like shape, a transform which is sensitive to the line patterns is highly useful. In addition, the integration along the line partially averages the speckle noise (see extraction algorithm described in Fig. 2).

Figure 3(a) shows the RT domain for the input image. Each point (ρ,θ) in the RT domain represents a single line in the x-y image domain. The location of the SPR dark line is represented by the local intensity minimum $g_{\min}(\rho,\theta)$ in the RT domain designated by an arrow in Fig. 3(a). However, additional minimal points may occur due to: a. noisy image, b. different shapes, and c. nonuniform illumination. This will lead to inaccuracy in the recognition of the desired local minimum. Additional unwanted minimal areas (obtained due to noisy image) will not be well defined and can be treated as a background. A background suppression technique needs to be carried out in order to suppress the unwanted minima, a common technique in sonar image processing for target detection.[13] The background suppression involves subtracting an estimated background using a 31×31 median filter operator ($MF^{31\times31}$) [Fig. 3(b)] from the

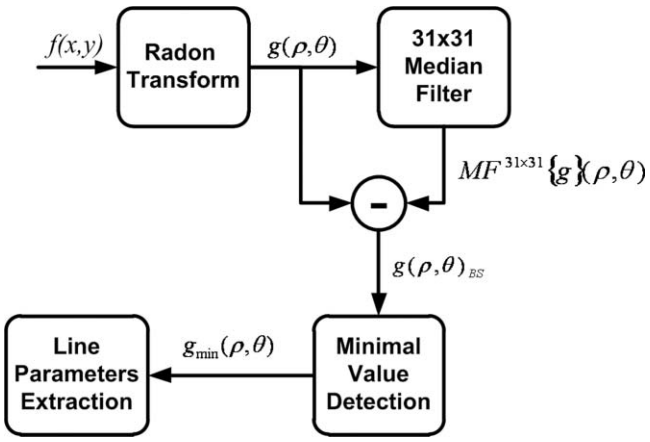

Fig. 2 Schematic diagram for extraction algorithm 1.

Radon transform image [Fig. 3(a)]. A result after background suppression (BS): $g(\rho,\theta)_{\mathrm{BS}}$ is shown in Fig. 3(c), and can be described by the following formula:

$$g(\rho,\theta)_{\mathrm{BS}} = g(\rho,\theta) - \mathrm{MF}^{31\times 31}\{g\}(\rho,\theta). \tag{2}$$

Figure 3(d) shows the line position (solid line along the image) using the proposed algorithm.

3.2 SPR Multichannel Extraction Algorithm

In the multichannel setup, a CCD sensor is aligned with the laser beam; therefore all the lines produced by the SPR are horizontally aligned. This fact enables usage of simple integration (summation in digital case) of the image along the y direction (n dimension of the CCD). Full RT is computationally complex, since it integrates along variety of angles as it can be seen from Eq. (2) and implementation of RT which is shown in Fig. 3(a). In the case when all lines

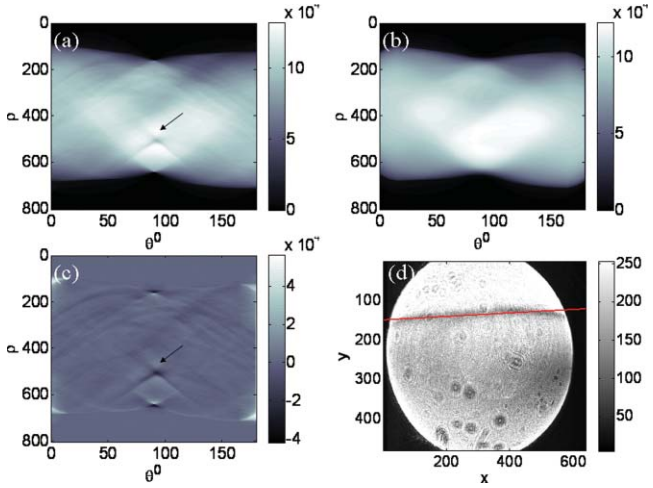

Fig. 3 (a) RT of original image: $g(\rho,\theta)$, (b) background: $\mathrm{MF}^{31\times 31}\{\mathrm{g}\}(\rho,\theta)$, (c) background suppression: $g(\rho,\theta)_{\mathrm{BS}}$. Note: the arrow marks minima which relates to the searched line in the image domain. (d) SPR image: $f(x,y)$ with a recognized SPR location designated by solid line along the image.

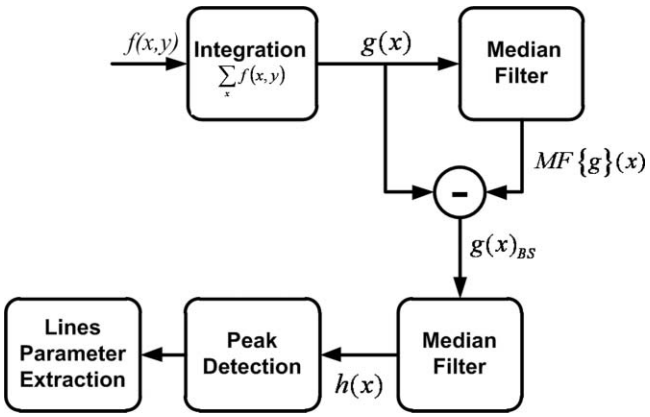

Fig. 4 Schematic diagram for extraction algorithm 2.

produced by the SPR are aligned, the problem can be reduced to the one-dimensional RT by integrating along the single θ:

$$g(x) = \sum_{u} f(u, x). \tag{3}$$

The lines produced by SPR will appear as local minima after the integration $g(x)$. Due to the imaging geometry and noise, additional minima can exist after the integration. The algorithm is shown schematically in Fig. 4. We have used a technique known as background suppression by subtracting a median filtered signal MF$\{g\}(x)$ from the integration output $g(x)$ (Fig. 5). The median filter size was chosen to be more than the peak width in order not to include them in background calculation [Eq. (2)].

For peak extraction, a zero crossing detection of the first derivative is used. After smoothing the signal using median filter, its first derivative is taken, which appears as a green line in Fig. 5. Points at the first derivative that exceed the slope threshold are treated as peaks. At the last stage of the algorithm, the highest peaks are selected (indicated by the vertical lines in Fig. 5.

We implemented this algorithm and checked it on triple channel SPR imaging sensing. The three channels were obtained by dividing the silicon isolator bath (component h in Fig. 1) into tree parts. Figure 6(a) shows a three channel imaging sensor, while each dark line relates to the SPR excitation at different analytes: oil of RI = 1.44, glue of the silicone isolator bath, and deionized (DI) water. Figure 6(b) shows extraction of the locations of the SPR lines.

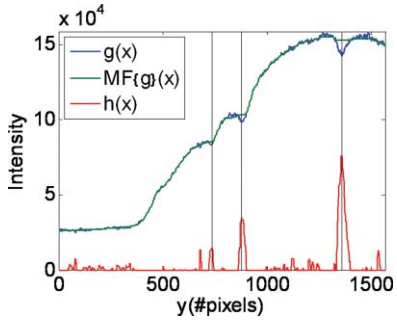

Fig. 5 SPR lines (Fig. 6) detection steps: $g(x)$ is integrated image (thin curve), MF$\{g(x)\}$ is median filtered integrated image (thick curve), and $h(x)$ is median filtered image (lower curve) after background suppression, while SPR line locations pointed by vertical lines. Extraction algorithm is described in details in Fig. 4.

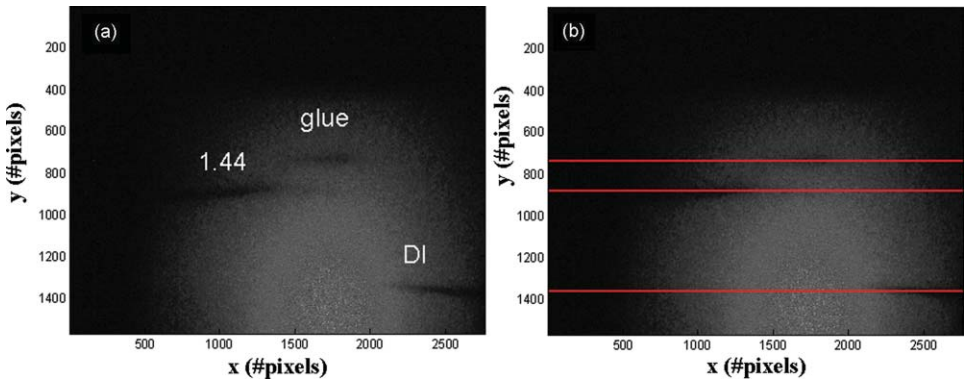

Fig. 6 Triple channel SPR imaging: RIs are 1.44, glue and DI abbreviates deionized water (RI of 1.3325): (a) original image in gray color map, and (b) processed image with extracted locations of SPR lines.

4 Thiolization of the Samples

In the 1980s, it was discovered that alkanethiols spontaneously assemble on noble metals.[14] Molecular self-assembly or self-assembly monolayer (SAM) is the assembly of molecules without guidance or management from an outside source.[15] SAM formation occurs in two steps. The initial step is very fast and includes an adsorption at the liquid–liquid, liquid–vapor, and liquid–solid interfaces. At the second step, which is much slower, monolayer organization of 2 to 4 nm thickness occurs. Monolayer formation is driven by a strong coordination of sulfur with the metal, accompanied by van der Waals interaction forces between the alkyl chains.[16] With a sufficient chain length (number of carbons), the resulting monolayer forms a densely packed and very stable structure that is oriented in case of alkanethiols approximately 36° to the noble metal surface.

Due to its stability to water environment and simple bio-immobilization protocol, gold is usually used as an SPR biosensing metal nanolayer.[16] By placing gold into a millimolar solution of an alkanethiol in ethanol, bio-surfaces can be created for any desired chemistry. However, poor attachment of gold to the glass substrate needs an additional layer of a few nanometers of Cr or Ti, which deform the SPR reflectivity versus angle curve. Silver, unlike gold, adheres very well to the glass. It has a very sharp curve, but silver is oxidizing when introduced to water or air medium, therefore, a thin protective layer (<15 nm) is needed to prevent oxidation. We used dense and packed thiol [11-mercaptoundecanoic acid (MUA)] – (Sigma product), layer which protects the silver from oxidation. The glass slides with deposited silver on them were immersed for 24 h in MUA, which was dissolved in dimethoxy-sulfoxide (DMSO) but not ethanol, under nitrogen atmosphere. We checked experimentally, that by using ethanol, an aggregated thiol layer on silver is achieved. Usage of an inorganic solution such as DMSO instead of ethanol is essential to enable a well-formed monolayer. Thiolization enables further immobilization of antigen for bio-specific sensing.

5 Application of the Single-Channel Extraction Algorithm–Chemosensor

Ethanol was diluted in water according to the known data.[17] Figure 7 presents RIs versus diluted ethanol in water (dotted curve), together with polynomial fit (solid curve):

$$y(z) = -0.00092z^5 + 0.0018z^4 + 0.0012z^3 - 0.0083z^2 + 0.014z + 1.4, \quad (4)$$

where $z = (c-39)/32$, c is a percentage of the ethanol diluted in water.

Some of the experimental results of the chemosensor (diagnosis of the changes in percent ethanol in water) are shown in Fig. 8. Note: we slightly changed the set-up depicted in Fig. 1

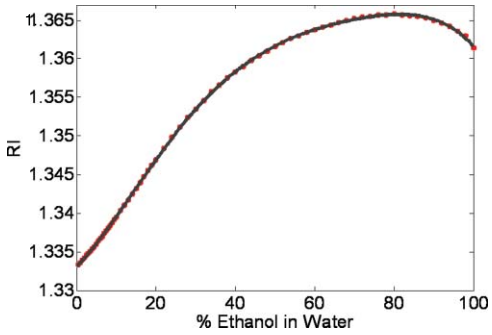

Fig. 7 RI as a function of ethanol concentrations c in water in percent (Ref. 17) (dotted curve) and its polynomial fit $y(z)$ (solid curve) according to Eq. (3).

by guiding the laser light with multimode optical fiber for homogenization of the beam. 70 nm Ag was deposited on the SF11 glass, and after that the samples [Fig. 8(a)] were immediately thiolated as it was described in Sec. 4, to prevent the silver from oxidation and enable further immobilization of the antigens.

The extracted location of the SPR line (in degrees) pattern using the described single channel extraction algorithm is shown in Fig. 9, which shows extracted SPR line locations as a function of the analyte RIs.

6 Sensitivity of the Sensor

The sensitivity of the sensor, which is evaluated from the regression line estimation, is $\Delta\phi^{\circ}/\Delta n = 60.79$ deg/RIU. Theoretical calculations give 61.74 deg/RIU sensitivity for the given parameters of the sensor (RIs of the analyte, SF11 prism, and the metal for incident wavelength of 637 nm) used in the SPR imaging sensor. To be able to analyze the sensitivity of the proposed sensor, it is necessary to know the angular position of the SPR line and the angular pixel size.

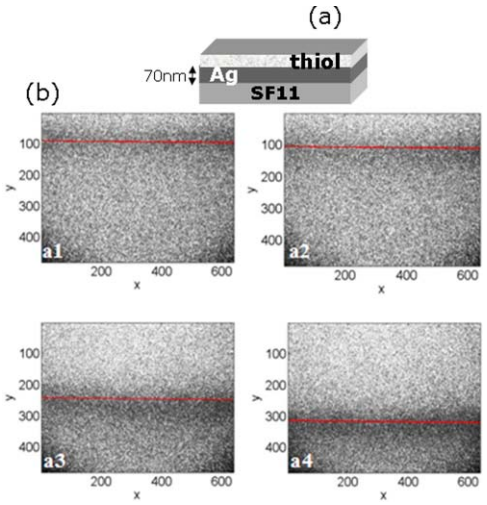

Fig. 8 (a) Implemented structure; (b) some of the experimental results of the SPR imaging: ethanol diluted in DI solutions: (a1) 100% DI, (a2) 10% ethanol in 90% DI, (a3) 40% ethanol in 60% DI, and (a4) 100% ethanol.

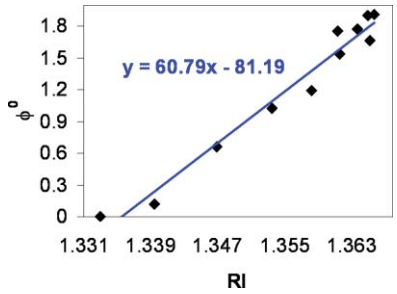

Fig. 9 Locations of the resonances achieved experimentally as a function of the RI of ethanol concentrations diluted in water (Ref. 17) and estimated regression line.

The angular shift in degrees $\Delta\phi^{\circ}$ is defined as follows:

$$\Delta\phi^{\circ} = \frac{\Delta p \delta\phi}{n}, \tag{5}$$

where Δp is the shift in pixels of the dark line with respect to the reference line (in our case DI water). $\delta\phi = D_{\text{lens}} \cdot \text{NA}/(D_{\text{spot}} \cdot n)$ is the angular pixel size in degrees: D_{lens} is the diameter of the lens [see Fig. 1(e)], D_{spot} is the diameter of the spot incident on the lens normal to the SPR line, NA is the numerical aperture of the fiber (here 0.55), and n is the dimension of the camera normal to the SPR line (the camera used by us has $m \times n = 659 \times 494$ pixels). Hence, the pixel size in our case is $\delta\phi = 0.0078^{\circ}$. The limit of detection (LoD), or the resolution of the sensor, is determined by the ratio between the noise level and the sensitivity: $\text{LoD} = \langle\delta\phi\rangle/\text{S}_{\phi}$ where $S_{\phi} = \Delta\phi/\Delta(\text{RI})$ is the angular sensitivity. Since the line is composed of m data points (pixels), and the minimum detectable angular shift is determined by the noise level which is a single pixel that corresponds to $\delta\phi = 0.0078^{\circ}$, the LoD is given by:

$$\text{LoD} = \frac{\delta\phi}{\sqrt{m}} \left(\frac{\Delta\phi}{\Delta(\text{RI})}\right)^{-1}. \tag{6}$$

Experimentally, the estimated LoD is 5×10^{-6} RIU. Note that the fact that we have a line composed of m pixels, improves our accuracy by a factor of $\sqrt{m}$. This is another advantage of the present technique over the standard angular scanning SPR technique or the SPR imaging technique with collimated beam.[18] A nanoprecision is achieved due to the fact that many data points (pixels) are used to determine the SPR location. To achieve the ideal LoD, one can optimize the system further such as using more divergence of the beam and using a camera with a larger number of pixels to decrease the pixel size. One can also use inverse scattering approaches such as theoretical calculation of reflectivity versus incidence angle, and fit it with experimental results[19] or parabolic fit near the dip minimum to achieve sub-pixel resolution.[20]

7 Lateral Resolution of the Sensor

The miniaturization of optics into subwavelength dimensions is of great current interest, as manipulating light fields on the nanoscale might be of major importance for future integrated optical devices, and especially biosensors. In multichannel sensing, one would like to minimize the sensing area in order to be able to increase the number of channels. Therefore, the smallest linear separable and measurable feature on the imaged surface is of high importance. For this purpose we checked the lateral resolution which is a measure of the ability of the sensor to detect closely separated objects such as SPR signals from the adjacent channels. The propagation length that a SP wave paths along the interface, between the dielectric and metal thin film, is defined by the decay length L_x which is usually dictated by the losses in the metal and can be regarded as a conservative measure of the spatial measurement resolutions on the imaging plane.[6] The

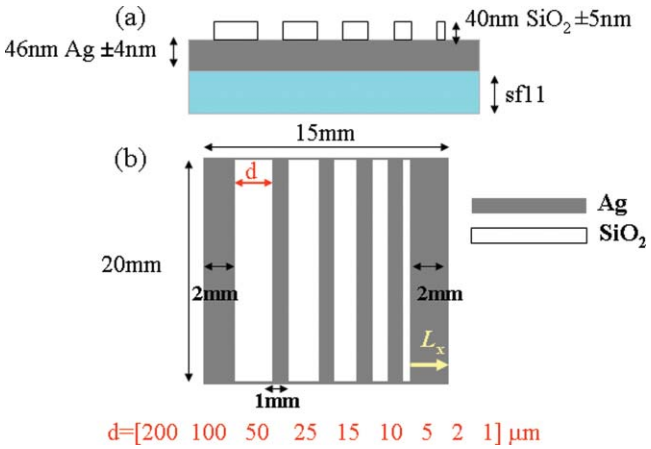

Fig. 10 Schematics of the sample configuration for measurement of the sensor lateral resolution. SiO_2 lines which have RI at 637 nm of 1.4569 on silver deposited on SF11 glass: (a) side and (b) top views of the designed structure.

decay length is the distance along the surface where the attenuation of the plasmon field occurs is proportional to ℓ/e or equivalently:

$$L_x = \frac{1}{2k_x''} = \frac{\lambda}{2\pi} \cdot \frac{\varepsilon_{mr}^2}{\varepsilon_{mi}} \cdot \left[\frac{\varepsilon_a + \varepsilon_{mr}}{\varepsilon_a \cdot \varepsilon_{mr}}\right]^{3/2}, \tag{7}$$

where k_x'' is the imaginary part of the complex SP wave vector, $k_x = k_x' + ik_x''$, ε_{mr}' and ε_{mi}'' are the real and imaginary parts of the dielectric function of the metal, that is $\varepsilon_m = \varepsilon_{mr}' + i\varepsilon_{mi}''$, while ε_a is the dielectric function of the analyte. Silver is the metal with the lowest losses in the visible spectrum. Its propagation distances L_x are typically in the range 10 to 100 μm.[21]

In order to check the propagation length of our sensor, we designed and fabricated a sample which is depicted in Fig. 10. After cleaning the glass slides, SiO_2 was sputtered on evaporated silver. The pattern of SiO_2 lines with different widths d and thickness of 40 nm were written using a laser writer (DWL 200) on silver of 46-nm thickness. At the final step, an RIE etch was done with the rate of 20 nm/min and the resist was removed. Figure 11 shows images of the fabricated sample with an achieved linewidth d slightly different from the design. Using a p-polarized diverged laser light, we achieved the image shown in Fig. 12. It is clear that on switching to an s-polarized light or rotating the prism out of the resonance angle range for either silver-air or Ag-SiO_2-air (indicated by the white arrows), SP excitation of the line patterns, which are in

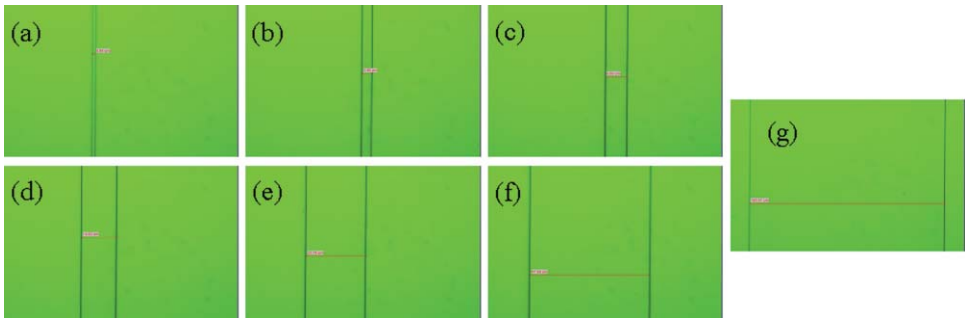

Fig. 11 Images from optical microscope of the sample depicted on Fig. 10, with linewidth d as follows: (a) 0.85 μm, (b) 3.9 μm, (c) 8.66 μm, (d) 14.02 μm, (e) 23.78 μm, (f) 47.68 μm, and (g) 195.57 μm.

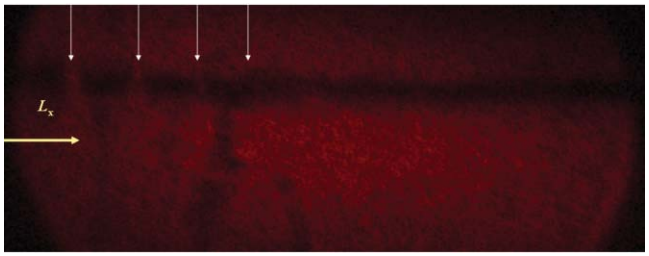

Fig. 12 SPR image of the patterned surface of the SiO_2 layer on top of the Ag layer obtained using of the setup depicted in Fig. 1 (without elements *f* and *j*).

Fig. 12 indicated by arrows, disappear. It can be seen from Fig. 12 that the resolution of the sensor is limited by 47.68 μm. Theoretically, the value should be comparable to $L_x \approx 9$ μm but it is believed that the silver layer is not ideal and grainy films are usually grown. Rothenhausler and Knoll[4] showed that the surface structure consisted of SiO_x stripes 9.3-nm thick and a 40-μm wide line imaged prepared by evaporation using an electron microscopy grid (slotted: 300 mesh) as a mask on 50 nm silver. Our results are close to this finding, but both are different from the theoretically expected value. Perhaps ultrasmooth silver films can help obtain a better resolution.

8 Conclusions

As an SPR line position detector, the use of the proposed Radon transform algorithm shows nanoprecision accuracy in cases of single and multichannel sensing. The method also provides the filtered output of the signal without any extra modification, and therefore, it is nonsensitive to the noise. Experimental results have confirmed the validity of the algorithm and its high precision in extracting the location of SPR lines from noisy images with very low contrast. Multichannel sensing was demonstrated using the same imaging approach and the use of the Radon transform with improved detection limit. The technique was also used to find the lateral resolution of the sensor using a patterned layer of 40-nm thick SiO_2 layer on top of the metallic surface. The technique proposed adds as a potential sensitivity enhancement method in SPR sensing.[22]

Acknowledgments

This work was supported by the Ministry of Science under Tashtiot program. We acknowledge Mr. Lev Tsapovsly and Professor Robert Marks from the Biotechnology Engineering Department for help in preparing an 11-MUA based solution for preventing silver samples from oxidation. We are grateful to Benny Hadad and Erez Golan from The Weiss Family Laboratory for Nanoscale Systems at BGU for their help during the fabrication of the nanostructure.

References

1. F. Blais and M. Rioux, "Real-time numerical peak detector," *Real-time numerical peak detector* **11**, 145–155 (1986).
2. I. Abdulhalim, M. Zourob, and A. Lakhtakia, "Surface plasmon resonance for biosensing: A mini-review," *Electromagnetics* **28**, 214–242 (2008).
3. H. Raether, *Surface Plasmons on Smooth and Rough Surfaces and on Gratings (Springer Tracts in Modern Physics)*, Vol. 111, Springer-Verlag, Berlin (1988).
4. B. Rothenhausler and W. Knoll, "Surface–plasmon microscopy," *Nature (London)* **332**, 615–617 (1988).
5. G. Steiner, "Surface plasmon resonance imaging," *Anal. Bioanal. Chem.* **379**, 328–331 (2004).

6. K. D. Kihm, "Surface plasmon resonance reflectance imaging technique for near-field (∼100 nm) fluidic characterization," *Exp. Fluids* **48**, 547–564 (2010).
7. K. S. Johnston, K. S. Booksh, T. M. Chinowsky, and S. S. Yee, "Performance comparison between high and low resolution spectrophotometers used in a white light surface plasmon resonance sensor," *Sens. Actuators B* **54**, 80–88 (1999).
8. C. J. Jacobus and R. T. Chien, "Two new edge detectors," *IEEE Trans. Pattern Anal. Mach. Intell.* **PAMI-3**, 581–592 (1981).
9. K. S. Johnston, S. S. Yee, and K. S. Booksh, "Calibration of surface plasmon resonance refractometers using locally weighted parametric regression," *Anal. Chem.* **69**, 1844–1851 (1997).
10. T. M. Chinowsky, L. S. Jung, and S. S. Yee, "Optimal linear data analysis for surface plasmon resonance biosensors," *Sens. Actuators B* **54**, 89 (1999).
11. A. Karabchevsky, S. Karabchevsky, and I. Abdulhalim, "Fast surface plasmon resonance imaging sensor using Radon transform," *Sens. Actuators B* **155**, 361–365 (2011).
12. S. Helgason, *The Radon Transform*, 2nd ed., Vol. 5. Series in Mathematics, Birkhauser Boston, c/o Springer-Verlag, New York (1999).
13. M. J. Chantler and J. P. Stoner, *Automatic Interpretation of Sonar Image Sequences Using Temporal Feature Measures: Special Issue on Image Processing for Oceanic Applications*, Vol. 22, Institute of Electrical and Electronics Engineers, New York, NY (1997).
14. R. G. Nuzzo and D. L. Allara, "Adsorption of bifunctional organic disulfides on gold surfaces," *J. Am. Chem. Soc.* **105**, 4481–4483 (1983).
15. C. D. Bain, E. B. Troughton, Y. T. Tao, J. Evall, G. M. Whitesides, and R. G. Nuzzo, "Formation of monolayer films by the spontaneous assembly of organic thiols from solution onto gold," *J. Am. Chem. Soc.* **111**, 321–335 (1989).
16. J. Homola, S. Löfås, and A. McWhirter, "The art of immobilization for SPR sensors," *Springer Series on Chemical Sensors and Biosensors* **4**, 117–151 (2006).
17. R. C. Weast and M. J. Astle, *Handbook of Chemistry and Physics*, Vol. 57, CRC Press, Boca Raton, FL (1979).
18. J. D. Swalen, J. G. Gordon, M. R. Philopott, A. Brillante, I. Pockrand, and R. Santo, "Plasmon surface polariton dispersion by direct optical observation," *Am. J. Phys.* **48**, 669–672 (1980).
19. I. Abdulhalim, M. Auslender, and S. Hava, "Resonant and scatterometric grating-based nanophotonic structures for biosensing," *J. Nanophoton.* **1**, 011680 (2007).
20. A. Lahav, A. Shalabaney, and I. Abdulhalim, "Surface plasmon sensor with enhanced sensitivity using top nano dielectric layer," *J. Nanophoton.* **3**, 031501 (2009).
21. W. L. Barnes, A. Dereux, and T. W. Ebbesen, "Surface plasmon subwavelength optics," *Nature (London)* **424**, 824–830 (2003).
22. A. Shalabney and I. Abdulhalim, "Sensitivity-enhancement methods for surface plasmon sensors," *Laser Photonics Rev.* (in press).

Alina Karabchevsky received her BSc and MSc in biomedical engineering from the Ben-Gurion University (BGU) of the Negev, Beer-Sheva, Israel in 2005 and 2008, respectively. During her MSc studies she specialized in biomedical signal processing. Currently, she is finalizing her 3rd year of PhD studies in electro-optics engineering at BGU. Recently she organized the SPIE student chapter at BGU and is acting as its first president. She has published 7 journal articles, coauthored another 3 journal articles and 1 conference proceeding paper, and made 12 conference presentations. Her research interests are in plasmonic nano-structures and optical biosensing devices, combining her biomedical engineering background with signal processing, electro-optics, and physics.

Serge Karabchevsky received his BSc in electrical and computer engineering from the Ben-Gurion University of the Negev, Beer-Sheva, Israel, in 2005. He spent several years working in the industry at companies such as BATM Telecom and GIDEL. Currently he is studying for an MSc in electro-optics engineering at Ben Gurion University, Beer-Sheva, Israel. His research interests are FPGA algorithms architecture, image processing, and autonomous robotics.

Ibrahim Abdulhalim studied physics at the Technion, Haifa, where he received his BSc, MSc, and DSc degrees in 1982, 1985, and 1988, respectively. He spent over 15 years working in applied optics in academia and industry including the University of Colorado at Boulder, the ORC at Southampton University, the University of Western Scotland, KLA-Tencor Corporation, Nova Measuring Instruments, and GWS-Photonics. In October 2005 he joined the Ben Gurion University, Department of Electro-Optic Engineering which he has been heading for four years. His current research activities involve nanophotonic structures for biosensing, liquid crystal devices, improved biomedical optical imaging techniques such as spectropolarimetric imaging, and full field optical coherence tomography. He has published over 100 journal articles, 50 conference proceedings papers, and 10 patents. He became a fellow of the Institute of Physics, UK in 2004 and recently he became a fellow of SPIE. He has been an associate editor of the SPIE Journal of Nanophotonics for 5 years and is on the editorial board of the Journal of Physics Express.